

## Article

# Formation of Late Paleoproterozoic Gaositai Hornblendite in Northern North China Craton: Evidence from Zircon U-Pb Isotopes and Amphibole Trace Elements

Taichang Zhu <sup>1,2</sup>, Zhiwei Wang <sup>1,2,\*</sup>, Zhihui Wang <sup>1,2</sup>, Yuxin Sun <sup>1,2</sup>, Zhenyu Liu <sup>1,2</sup>, Yin Xu <sup>1,2</sup>, Jingwen Yu <sup>1,2</sup>, Hao Wei <sup>3</sup> and Xiaolei Geng <sup>4</sup>

<sup>1</sup> Hebei Key Laboratory of Strategic Critical Mineral Resources, Hebei GEO University, Shijiazhuang 050031, China

<sup>2</sup> College of Earth Sciences, Hebei GEO University, Shijiazhuang 050031, China

<sup>3</sup> Geological Testing Center, Hebei GEO University, Shijiazhuang 050031, China

<sup>4</sup> Hebei Institute of Geological Survey, Shijiazhuang 050000, China

\* Correspondence: wangzw14@mails.jlu.edu.cn or wangzw@hgu.edu.cn; Tel.: +86-311-8720-8285

**Abstract:** Paleoproterozoic tectonic evolution of the northern North China Craton has been a hot research topic. We firstly identified a 1.85 Ga hornblendite from the Gaositai mafic–ultramafic complex, in northern Hebei. Systematic studies of petrology, zircon U-Pb geochronology, and in situ mineral major and trace elements of hornblendite are the key to revealing the petrogenesis of the Paleoproterozoic ultramafic rock and the tectonic evolution of northern North China Craton. LA-ICP-MS zircon U-Pb dating suggests the Gaositai hornblendite formed at  $1851 \pm 44$  Ma. The late Paleoproterozoic ultramafic rocks, together with coeval post-collisional granites, formed a bimodal igneous assemblage. Both hornblende and its equilibrium melt compositions show strongly fractionated HREE patterns, relative enrichments in LREEs and LILEs, and depletions in HREEs and HFSEs. The phlogopite-bearing hornblendite magma could have originated from a hydrous garnet-facies mantle source metasomatized by slab-derived silicate melt. Furthermore, the variations of major and trace elements in hornblende from core to rim also reveal the mineral fractional crystallization and magma recharge. Zircon trace elements, melt composition equilibrium with hornblendes, and the bimodal igneous assemblage suggest that the generation of the Gaositai Paleoproterozoic hornblendite was likely the product of post-collisional extension related to the collision between eastern and western North China blocks.



**Citation:** Zhu, T.; Wang, Z.; Wang, Z.; Sun, Y.; Liu, Z.; Xu, Y.; Yu, J.; Wei, H.; Geng, X. Formation of Late Paleoproterozoic Gaositai Hornblendite in Northern North China Craton: Evidence from Zircon U-Pb Isotopes and Amphibole Trace Elements. *Minerals* **2022**, *12*, 1046. <https://doi.org/10.3390/min12081046>

Academic Editor: Rubén Díez-Fernández

Received: 15 July 2022

Accepted: 17 August 2022

Published: 19 August 2022

**Publisher's Note:** MDPI stays neutral with regard to jurisdictional claims in published maps and institutional affiliations.



**Copyright:** © 2022 by the authors. Licensee MDPI, Basel, Switzerland. This article is an open access article distributed under the terms and conditions of the Creative Commons Attribution (CC BY) license (<https://creativecommons.org/licenses/by/4.0/>).

## 1. Introduction

The North China Craton (NCC), one of the oldest and largest Precambrian cratons in China, develops the Archean to Paleoproterozoic crystalline basement, and Meso- to Neoproterozoic and Paleozoic sedimentary cover (Figure 1a). The NCC is a key object for studying the Precambrian tectonic regime transformation, evolution of supercontinents, and continental crust [1–17]. However, there is still a significant amount of disagreement regarding the timing of cratonization and the Paleoproterozoic tectonic evolution. For instance, some scholars believe that the North China Craton's basement was created by numerous blocks colliding at 2.7–2.5 Ga, with rifting taking place throughout the Paleoproterozoic, and the blocks colliding once more at 1.95–1.85 Ga [15,18–20]. Another theory holds that the Yinshan and Ordos blocks, and the Longgang and Langrim blocks, amalgamated at 1.95 Ga and 1.90 Ga, respectively, to form the Western and Eastern blocks, and the oceanic crust was long-term subducted beneath the two blocks, but there were different understandings of subduction polarity. The Western and Eastern blocks ultimately collided together along the Trans-North China Orogen (TNCO) in 1.85 Ga, which coincided

with the formation time of other major cratons throughout the world, representing the assembly of the Columbia supercontinent [3,4,8,21–25].

Neoarchean–Paleoproterozoic geological records are well-developed in the northern Hebei region of the NCC (Figure 1b); the predecessors focused mainly on the formation and metamorphic ages of the Neoarchean metamorphic complex, and petrogenesis of ~2.5 and 1.8 Ga metavolcanic rocks and granitoids, revealing the Neoarchean subduction and Paleoproterozoic collision to extension processes [9,13,25–30]. Traditionally, it has been assumed that there are large areas of Paleoproterozoic mafic–ultramafic rocks in the northern Hebei region, such as the Gaositai mafic–ultramafic complex, Damiao anorthosite, etc. [31]. Numerous studies have concluded that the Damiao anorthosite generated at 1.74 Ga, which was the product of post-collisional extension [24]. While the Gaositai mafic–ultramafic complex was considered to be a 280 Ma Alaskan-type rock association (Figure 1c), associated with an extensional mechanism that has different interpretations of back-arc extension and intracontinental extension [32–34], some researchers have also proposed that the formation and mineralization age was 213 Ma [35].

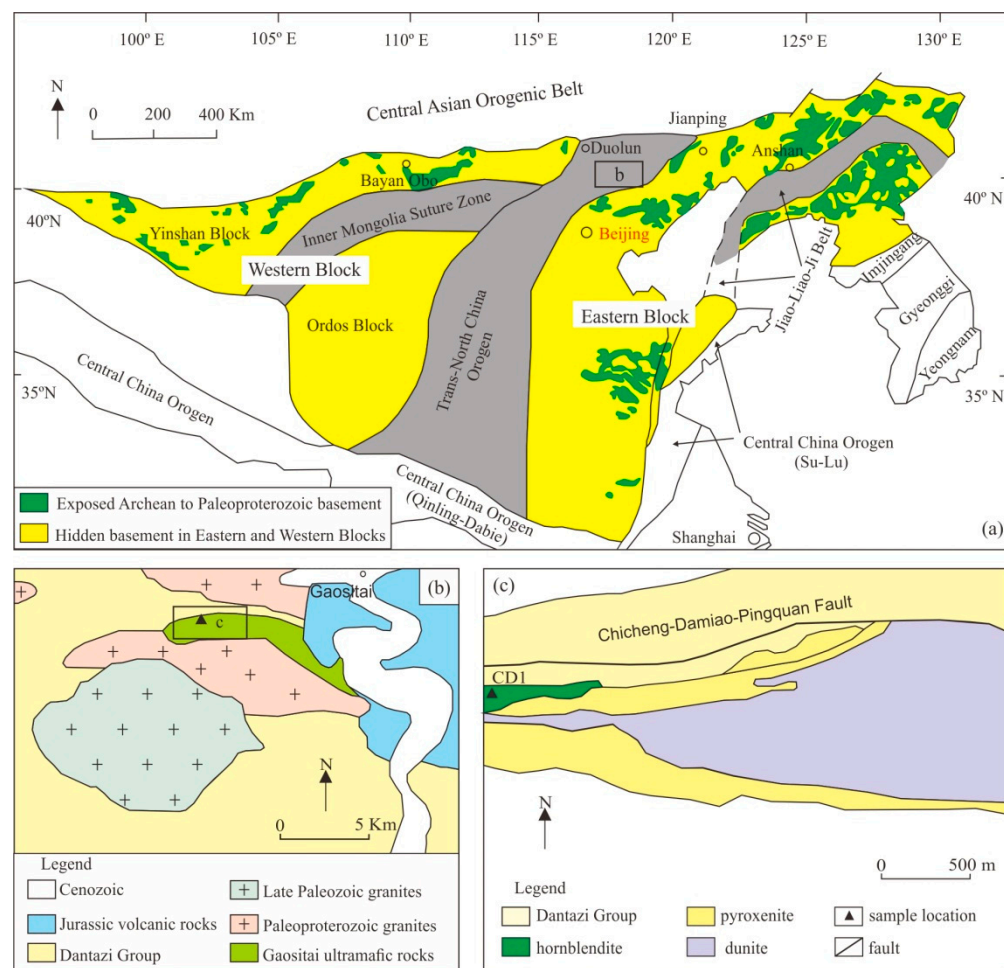


**Figure 1.** Tectonic subdivision of the North China Craton, modified from Zhao et al. and Santosh [21,23] (a); simplified geological map of the Gaositai area in Northern Hebei (b); and a detailed geological map of Gaositai mafic-ultramafic rocks, modified from Chen et al. [33] (c).

Fortunately, we discovered a 1.85 Ga hornblendite (CD1) from the Gaositai mafic-ultramafic rocks for the first time (Figure 1c). Previous studies have shown that magmatic zircons in hornblendites could record the formation age, zircon trace elements can be used to determine the tectonic setting, and the in situ major and trace element compositions of hornblendes and their equilibrium magma can reveal the nature of the primary magma and magma evolution [32,36–41]. Therefore, systematic petrology, zircon U-Pb dating, and in situ major and trace element analyses of hornblendite are the keys to revealing the petrogenesis of the Paleoproterozoic ultramafic rock and the geodynamic mechanism of the northern NCC.

## 2. Geological Setting and Sampling

The Gaositai area in northern Chengde is situated at the northernmost Trans-North China Orogen (TNCO), in the northern part of NCC (Figure 1a), and has developed a large area of Archean supracrustal rocks, granitic gneisses, Mesoproterozoic mafic rocks, and Late Paleozoic mafic-ultramafic rocks. The supracrustal rocks are represented by the Dantazi Group and the Hongqiyizingzi Group. The former group is mainly distributed south of the Chicheng-Damiao-Pingquan fault, and the rock association includes trondhjemite-tonalite-granodiorite (TTG), mafic granulite, amphibolite, garnet-biotite schist, and marble. The latest research has determined that the formation ages of the TTG were Neoarchean to Paleoproterozoic (2.6–2.4 Ga), and most rocks in this group have undergone 2.4, 1.9–1.8 Ga granulite-amphibolite facies metamorphism [25,27,28]. The Paleoproterozoic Hongqiyizingzi Group is distributed north of the fault, overlaid on the Dantazi Group in an angular unconformity, and the rock assemblage is gneiss, quartzite, mica schist, and marble. Liu et al. [9] recognized Neoarchean (2546–2532 Ma) quartz dioritic-tonalitic-granodioritic gneisses and Paleoproterozoic (1870–1819 Ma) granodiorite-monzo-granite-syenogranite intrusions from the Hongqiyizingzi Group, and some Late Paleozoic granites have been also identified from it [26]. Additionally, a small amount of 1894–1878 Ma S-type garnet granites occurred in Lanqi Town, Longhua, which is located north of the research region [29]. The Mesoproterozoic magmatic rocks include the Damiao 1742–1739 Ma anorthosite, mangerite, and minor troctolite [24]. Late Paleozoic mafic-ultramafic rocks also formed in Gaositai, Hongshila, and Bolouonuo regions, including the 393–381 Ma pyroxenites, amphibole pyroxenites, hornblendites, and gabbros, as well as the 297–280 Ma gabbros [32–34].

In this study, we conducted petrological studies on a hornblendite (CD1) from the western part of the Gaositai mafic-ultramafic complex (Figure 1c), which intruded into the Archean–Paleoproterozoic metamorphic and deformed supracrustal rocks. The hornblendite has a massive structure, inequigranular texture, and a mineral composition dominated by amphibole (90%), magnetite (6%), pyrite (2%), and phlogopite (2%) (Figure 2). Hornblende can be divided into two groups. One is coarse-grained with clinopyroxene, with magnetite inclusions in the cores and pyrite inclusions in the rims. The fine-grained hornblende crystals in the other group coexist with magnetites and pyrites (Figure 2c,d). Phlogopite appears between medium- to fine-grained hornblende grains (Figure 2c). According to these petrological characteristics, we infer that clinopyroxene firstly crystallized, then the core of coarse-grained hornblende and magnetite was generated, followed by the formation of the mantle to the rim of coarse-grained hornblende, medium-to fine-grained hornblende, magnetite, pyrite, and phlogopite.

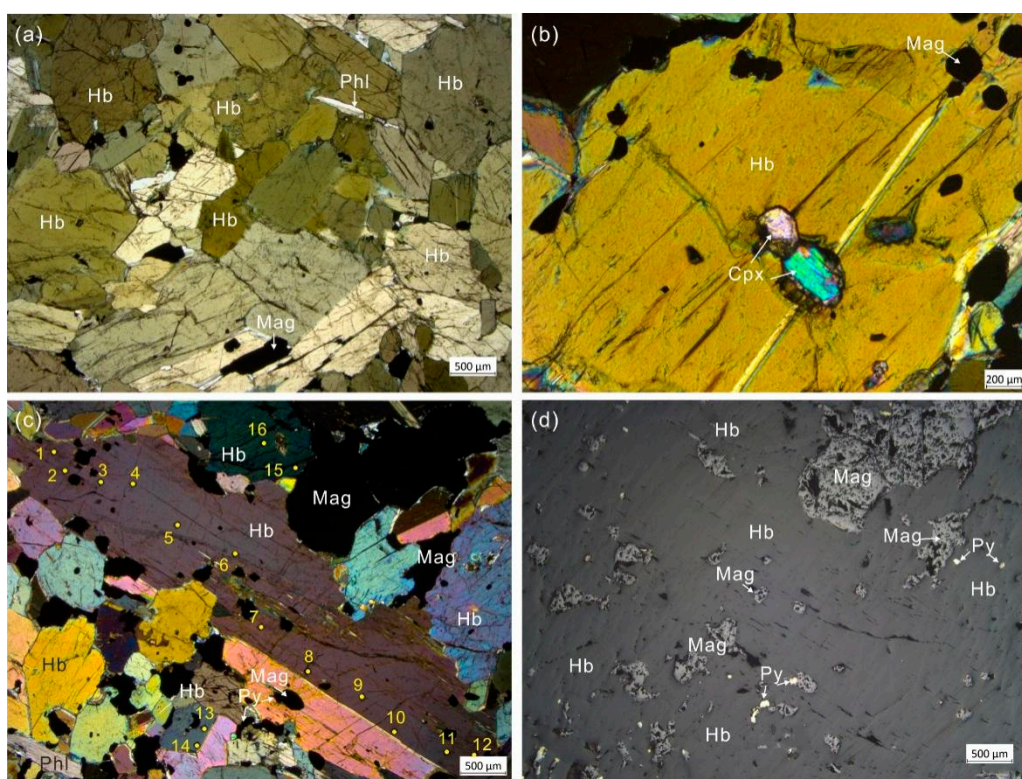


**Figure 2.** Photomicrographs of the Gaositai hornblendite. (a) Massive hornblendite, plane polarized light, (b) clinopyroxene and magnetite inclusions in hornblende, cross polarized light, (c) coarse- and fine-grained hornblendes, locations of in situ major and trace elements analyses, cross polarized light, (d) Magnetite and pyrite in hornblendite, reflected light. Cpx—clinopyroxene, Hb—Hornblende, Mag—magnetite, Phl—phlogopite, Py—pyrite.

### 3. Analytical Methods and Results

#### 3.1. Analytical Methods

Zircon U-Pb dating and trace element analysis were determined by laser ablation inductively coupled plasma mass spectrometry (LA-ICP-MS) at Hebei Key Laboratory of Strategic Critical Mineral Resources, Hebei GEO University. The instrument couples a quadrupole ICP-MS (iCAP RQ) and a 193-nm ArF Excimer laser (RESOlution-LR). Laser spot size was set to 29  $\mu\text{m}$ , laser energy density was 3 J/cm<sup>2</sup>, and the repetition rate was 6 Hz. A zircon 91500 standard was utilized for external age calibration, and a zircon GJ-1 standard was used as a secondary standard to monitor the deviation of age calculation. Calibrations for zircon trace element concentrations were performed using NIST SRM610 as an external standard and Si as the internal standard. Detailed instrumental conditions and data acquisition procedures were described by Wang et al. [42]. Data reduction was done using ICPMSDataCal and Isoplot (v.3.0) tools [43,44]. Isotope ratio and age uncertainties were quoted at the 1 sigma level. Zircon U-Pb dating and trace element results were given in Tables 1 and 2.

Major and trace element compositions for hornblende were determined by LA-ICP-MS at Hebei Key Laboratory of Strategic Critical Mineral Resources. Laser spot size was set to 61  $\mu\text{m}$ , laser energy was 100 mJ, and the repetition rate was 4 Hz. Data reduction was carried out by the iolite 4 software, using NIST SRM 610 as the external standard and Si as the internal one. NIST SRM612 was analyzed as a secondary standard quality control [45]. Major and trace element compositions of hornblende are reported in Table 3.

**Table 1.** LA-ICP-MS zircon U-Pb dating results for the Gaositai hornblendite.

Spot No.	Th	U	Th/U	Isotopic Ratios						Age(Ma)					
	ppm	ppm		$^{207}\text{Pb}/^{206}\text{Pb}$	1σ	$^{207}\text{Pb}/^{235}\text{U}$	1σ	$^{206}\text{Pb}/^{238}\text{U}$	1σ	$^{207}\text{Pb}/^{206}\text{Pb}$	1σ	$^{207}\text{Pb}/^{235}\text{U}$	1σ	$^{206}\text{Pb}/^{238}\text{U}$	1σ
CD1—1	173	403	0.4	0.1506	0.0014	9.6495	0.1201	0.4636	0.0046	2354	16	2402	12	2455	20
CD1—2	26	48	0.6	0.1143	0.0017	5.3101	0.1053	0.3361	0.0052	1869	28	1870	17	1868	25
CD1—3	86	165	0.5	0.1458	0.0016	7.4541	0.0998	0.3701	0.0047	2298	19	2167	12	2030	22
CD1—4	64	93	0.7	0.1334	0.0019	3.7232	0.1000	0.2019	0.0048	2144	24	1576	22	1186	26
CD1—5	69	159	0.4	0.1631	0.0011	9.4580	0.1478	0.4197	0.0062	2488	12	2383	14	2259	28
CD1—6	30	79	0.4	0.1550	0.0014	9.7285	0.2088	0.4523	0.0076	2402	15	2409	20	2406	34
CD1—7	13	31	0.4	0.1727	0.0028	11.8622	0.2651	0.4971	0.0081	2584	27	2594	21	2601	35
CD1—8	6	21	0.3	0.1553	0.0028	9.6571	0.2031	0.4519	0.0067	2405	30	2403	19	2404	30
CD1—9	92	304	0.3	0.1123	0.0010	3.9049	0.0520	0.2516	0.0028	1839	16	1615	11	1447	14
CD1—10	19	42	0.4	0.1664	0.0018	11.2507	0.2653	0.4895	0.0107	2522	17	2544	22	2568	46
CD1—11	13	36	0.4	0.1582	0.0022	9.6098	0.2085	0.4392	0.0070	2437	24	2398	20	2347	31
CD1—12	363	259	1.4	0.1393	0.0015	7.9324	0.1086	0.4120	0.0042	2218	19	2223	12	2224	19
CD1—13	14	30	0.5	0.1539	0.0028	9.5192	0.2111	0.4481	0.0092	2391	31	2389	20	2387	41
CD1—14	16	59	0.3	0.1420	0.0019	7.7669	0.1202	0.3958	0.0070	2254	24	2204	14	2150	32
CD1—15	207	213	1.0	0.1457	0.0013	7.6907	0.1215	0.3817	0.0047	2295	15	2196	14	2084	22
CD1—17	42	69	0.6	0.1379	0.0015	7.8090	0.0991	0.4109	0.0049	2211	19	2209	12	2219	22
CD1—18	25	67	0.4	0.1102	0.0020	5.4703	0.1637	0.3579	0.0070	1803	34	1896	26	1972	33
CD1—19	68	144	0.5	0.1327	0.0013	7.9135	0.1067	0.4319	0.0037	2200	17	2221	12	2314	17
CD1—20	83	156	0.5	0.1327	0.0013	7.7905	0.1002	0.4255	0.0041	2200	17	2207	12	2285	18

**Table 2.** LA-ICP-MS zircon trace element results (ppm) for the Gaositai hornblendite.

Spot No.	Y	Nb	La	Ce	Pr	Nd	Sm	Eu	Gd	Tb	Dy	Ho	Er	Tm	Yb	Lu	Th	U
CD1—1	251	2.51	0.03	21.6	0.13	0.45	0.88	0.17	4.89	1.45	18.1	7.79	36.7	9.73	105	21.3	173	403
CD1—2	162	2.48	0.03	14.6	0.02	0.70	1.26	0.56	3.83	1.18	15.0	5.55	25.9	6.39	66.2	14.7	26.3	47.5
CD1—3	286	1.25	0.00	14.9	0.07	0.74	1.18	0.18	5.67	1.95	25.9	8.95	42.2	11.1	112	21.6	86.3	165
CD1—4	327	1.43	0.25	14.4	0.65	2.28	1.81	0.26	6.71	2.39	29.4	10.7	49.0	11.7	118	21.6	63.9	92.8
CD1—5	225	1.24	0.00	13.0	0.07	0.39	0.79	0.15	3.68	1.44	18.5	7.14	34.5	9.14	98.6	18.8	68.7	159
CD1—6	244	0.70	0.00	10.8	0.04	0.24	0.86	0.20	4.35	1.49	19.9	7.91	37.6	9.91	104	20.1	29.8	78.5

**Table 2.** *Cont.*

Spot No.	Y	Nb	La	Ce	Pr	Nd	Sm	Eu	Gd	Tb	Dy	Ho	Er	Tm	Yb	Lu	Th	U
CD1—7	303	1.77	0.00	15.4	0.15	0.67	1.33	0.14	6.36	2.18	24.9	9.84	46.3	11.4	117	21.4	12.8	31.5
CD1—8	246	1.25	0.01	12.0	0.09	0.59	1.14	0.16	5.32	1.66	20.9	7.83	35.1	8.88	92.5	16.5	5.71	20.7
CD1—9	148	1.89	0.09	18.7	0.16	0.84	1.22	0.32	4.41	1.18	13.6	4.51	20.9	5.17	52.8	10.2	91.7	304
CD1—10	298	1.61	0.01	14.6	0.06	0.65	1.28	0.18	6.01	1.88	24.6	9.42	42.8	11.4	116	21.3	18.5	42.0
CD1—11	268	2.00	0.00	15.6	0.05	0.64	1.27	0.16	5.47	1.85	21.8	8.65	39.6	10.0	104	18.5	12.8	36.3
CD1—12	1278	2.70	0.06	35.0	0.25	2.62	6.21	0.78	34.3	9.93	120	43.3	179	40.7	358	65.1	363	259
CD1—13	259	1.28	0.00	13.0	0.07	0.48	1.38	0.18	5.22	1.81	22.7	8.39	37.2	9.71	100	18.3	14.4	29.7
CD1—14	316	0.96	0.02	13.3	0.06	0.48	1.12	0.16	5.10	1.94	23.5	9.68	46.1	13.0	144	25.9	15.9	59.0
CD1—15	970	1.77	0.04	24.9	0.50	4.71	8.33	0.56	29.3	8.31	98.7	32.9	136	31.8	287	48.3	207	213
CD1—17	1908	6.19	0.00	16.5	0.08	0.76	1.84	0.24	8.66	3.15	38.2	14.7	68.4	17.0	170	31.8	42.2	68.6
CD1—18	476	1.79	0.01	16.7	0.09	0.59	1.20	0.26	3.50	0.97	10.3	3.59	16.2	4.03	41.5	8.17	25.2	67.3
CD1—19	113	0.69	0.00	12.8	0.07	0.62	1.04	0.10	4.13	1.54	19.9	7.81	36.7	9.24	93.3	18.8	68.5	144
CD1—20	247	1.32	0.00	14.5	0.06	0.81	1.43	0.13	6.88	2.45	30.2	11.8	52.8	13.6	137	25.2	83.4	156

**Table 3.** Compositions (ppm) of amphiboles in the Paleoproterozoic Gaositai hornblendite.

Spot No.	HB-1	HB-2	HB-3	HB-4	HB-5	HB-6	HB-7	HB-8	HB-9	HB-10	HB-11	HB-12	HB-13	HB-14	HB-15	HB-16
Li	0.55	0.73	0.48	0.45	0.54	0.57	0.58	1.16	0.60	0.57	0.62	1.93	0.66	0.67	2.05	0.60
Na	15,962	16,635	16,083	16,075	16,317	16,444	16,620	17,714	16,556	16,423	16,138	16,643	15,921	15,940	17,521	16,338
Mg	67,686	67,899	67,035	67,534	66,956	67,414	67,957	68,057	67,456	67,129	67,351	65,937	68,305	67,943	66,843	67,998
Al	61,155	61,864	60,765	58,585	59,016	58,836	61,151	61,176	59,786	61,681	61,392	62,843	61,095	61,319	62,041	63,535
P	64.03	65.48	70.24	70.24	76.57	79.39	71.05	77.39	100.45	102.11	123.94	57.33	66.87	62.57	65.48	76.74
K	9777	9706	9549	8835	8721	8873	9249	8686	8571	9414	9882	10,931	10,090	10,078	9123	10,281
Ca	79,879	79,432	78,830	78,627	77,780	78,570	79,532	78,084	77,487	79,117	78,874	78,012	79,046	79,188	79,713	80,572
Sc	101	100	99.2	98.8	97.5	99.2	96.7	91.5	88.9	95.9	104	110	100	100	117	102
Ti	6046	6084	6237	6007	6095	6005	5942	5937	6077	6198	6149	6225	6053	6061	5708	6180
V	468	502	469	442	440	438	452	495	440	454	458	492	474	468	530	495
Cr	31.8	31.7	23.0	8.0	25.3	11.7	28.6	18.9	10.7	17.9	21.3	26.8	39.0	38.7	29.7	31.0
Mn	863	856	891	899	901	902	853	882	917	906	901	876	894	917	883	890

**Table 3.** Cont.

Spot No.	HB-1	HB-2	HB-3	HB-4	HB-5	HB-6	HB-7	HB-8	HB-9	HB-10	HB-11	HB-12	HB-13	HB-14	HB-15	HB-16
Fe	79,230	79,121	82,846	81,720	83,607	83,693	77,009	89,890	84,960	85,249	84,358	84,052	81,608	82,702	83,269	83,315
Co	55.8	53.9	57.1	57.3	57.9	58.4	54.0	57.4	58.8	58.1	59.7	56.7	56.6	56.1	56.9	57.7
Ni	24.1	23.6	23.2	21.8	22.3	20.9	23.8	61.9	24.1	24.0	25.8	26.5	25.0	24.8	32.1	26.6
Cu	0.55	0.85	0.51	0.47	1.22	0.61	0.82	758.41	0.65	0.76	2.50	2.81	0.69	0.52	0.68	0.53
Zn	54.3	55.9	55.4	57.7	55.8	58.5	56.9	65.0	58.0	58.3	59.1	64.0	57.0	55.4	77.5	56.8
Ga	14.4	14.6	13.7	13.5	14.0	13.7	14.1	15.7	14.0	14.2	13.9	15.3	14.2	14.4	16.0	14.7
Rb	3.73	4.03	3.67	3.03	2.98	2.90	3.39	3.96	3.10	3.68	4.04	6.67	4.11	3.87	4.55	4.08
Sr	387	386	377	348	353	349	389	374	360	386	386	396	377	378	374	402
Y	15.5	15.1	15.2	15.3	16.1	15.2	15.3	17.3	18.1	17.4	16.0	14.8	14.3	14.5	14.4	15.4
Zr	14.8	14.6	14.8	13.3	14.0	14.3	15.9	18.3	18.5	17.9	16.1	15.5	15.0	15.8	16.5	16.0
Nb	1.97	1.92	1.90	1.68	1.76	1.75	1.87	2.10	1.86	1.99	1.98	1.91	1.98	2.01	1.99	2.04
Sn	0.82	0.93	0.86	0.83	0.77	0.79	0.90	1.06	1.02	1.04	0.97	0.88	0.88	0.95	1.15	1.04
Ba	175	180	188	176	171	170	182	191	165	186	194	201	198	189	215	199
La	4.27	4.07	4.01	3.66	3.87	3.86	4.20	4.21	4.19	4.37	4.38	4.49	4.22	4.13	4.10	4.37
Ce	14.5	14.4	14.1	13.6	14.4	14.2	14.5	15.4	16.2	16.2	15.7	15.7	14.5	14.4	14.4	15.2
Pr	2.77	2.77	2.72	2.68	2.90	2.75	2.88	3.05	3.15	3.05	2.95	2.90	2.71	2.73	2.75	2.83
Nd	16.0	15.5	14.7	15.6	16.2	15.7	16.1	17.2	18.2	17.3	16.5	15.8	15.3	15.4	15.5	15.8
Sm	4.73	4.57	4.67	4.72	4.93	4.71	4.76	5.40	5.26	5.21	4.96	4.91	4.28	4.37	4.56	4.85
Eu	1.48	1.44	1.46	1.56	1.58	1.50	1.47	1.59	1.70	1.68	1.57	1.53	1.40	1.35	1.38	1.46
Gd	4.65	4.51	4.40	4.65	5.08	4.79	4.69	5.15	5.26	5.24	4.97	4.56	4.39	4.38	4.55	4.58
Tb	0.62	0.64	0.61	0.61	0.64	0.63	0.63	0.70	0.72	0.68	0.64	0.62	0.57	0.61	0.58	0.64
Dy	3.46	3.52	3.52	3.48	3.69	3.51	3.56	3.87	4.15	3.91	3.70	3.45	3.27	3.31	3.19	3.57
Ho	0.66	0.61	0.64	0.65	0.67	0.65	0.64	0.72	0.78	0.70	0.66	0.63	0.57	0.60	0.59	0.64
Er	1.64	1.70	1.66	1.62	1.64	1.61	1.59	1.85	1.99	1.74	1.68	1.58	1.60	1.44	1.38	1.63
Tm	0.20	0.18	0.19	0.19	0.20	0.20	0.20	0.21	0.23	0.23	0.21	0.20	0.18	0.18	0.18	0.18
Yb	1.09	1.04	1.10	1.11	1.30	1.21	1.14	1.42	1.49	1.31	1.07	1.09	0.99	1.02	1.01	1.08
Lu	0.15	0.15	0.13	0.15	0.16	0.15	0.15	0.18	0.18	0.07	0.17	0.16	0.14	0.13	0.13	0.14
Hf	1.12	1.07	1.09	1.03	1.10	1.04	1.26	1.39	1.44	1.39	1.23	1.15	1.10	1.12	1.19	1.09
Ta	0.08	0.08	0.07	0.06	0.07	0.06	0.08	0.08	0.06	0.07	0.08	0.08	0.08	0.09	0.08	0.09
Pb	0.72	0.80	0.76	0.72	0.77	0.76	0.77	1.56	0.74	0.81	0.81	0.87	0.73	0.76	0.75	0.85
Th	0.06	0.06	0.06	0.05	0.05	0.05	0.05	0.05	0.05	0.06	0.06	0.07	0.06	0.07	0.06	0.06
U	0.01	0.01	0.02	0.01	0.02	0.02	0.01	0.02	0.01	0.01	0.01	0.03	0.02	0.02	0.02	0.02

### 3.2. Analytical Results

#### 3.2.1. Zircon U-Pb Dating

Zircon grains in the Gaositai hornblendite exhibit distinct cathodoluminescence (CL) image properties, and the corresponding U-Pb dating results likewise reveal multi-stage ages (Figures 3 and 4a, Table 1). Three zircon grains, which range from subhedral to euhedral, exhibit oscillatory zoning and high Th/U ratios of 0.31–0.55, indicating a magmatic origin. Three analytical spots yield the youngest upper intercept age of  $1851 \pm 44$  Ma (MSWD = 1.4) (Figure 4a; the calculated error correlation value is 0.6), which can represent the Gaositai hornblendite's formation age. Another group of zircons mostly develops core-rim structures (Figure 3), and their inner cores with Th/U ratios of 0.27–1.4 show oscillatory zoning, which is of magmatic origin. However, their rims are zoneless, which points to a metamorphic origin. Seven spots of magmatic cores give an upper intercept age of  $2206 \pm 10$  Ma (MSWD = 1.01). In addition, there are seven surrounded to rounded zircon grains in the sample, which show weak oscillatory zoning and relatively high Th/U ratios of 0.28–0.49, further indicating that these magmatic zircons underwent later metamorphism. Eight analyses yield one concordant  $^{207}\text{Pb}/^{206}\text{Pb}$  age ( $2399 \pm 13$  Ma, MSWD = 0.17,  $n = 6$ ) and two older  $^{207}\text{Pb}/^{206}\text{Pb}$  concordant ages ( $2584 \pm 27$  Ma,  $2522 \pm 17$  Ma).

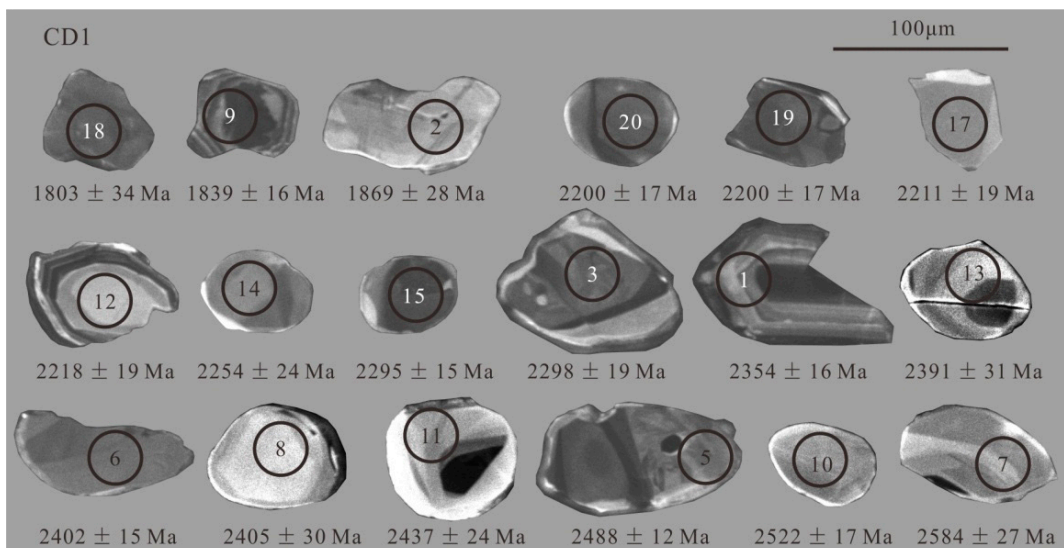


**Figure 3.** Zircon CL images of the Paleoproterozoic Gaositai hornblendite. Numbers in circles are analysis numbers.

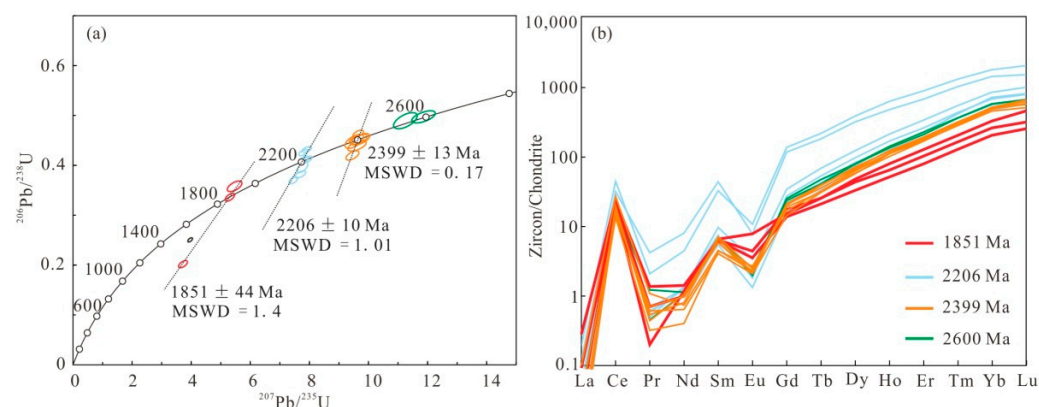


**Figure 4.** Zircon concordia diagram (a) and REE patterns [46] (b) of the Paleoproterozoic Gaositai hornblendite.

The chondrite-normalized zircon rare earth element (REE) patterns show light rare earth element (LREE) depletion, heavy rare earth element (HREE) enrichment, and positive Ce anomalies and negative Eu anomalies (Figure 4b), consistent with the features of most magmatic zircons. Given the high Th/U ratios of zircons, this indicates that metamorphism has not significantly affected the REE patterns of 2.4–2.6 Ga zircons. In addition, it is noted that 1.85 Ga magmatic zircons contain relatively lower contents of heavy REE than the older captured zircons (Figure 4b).

### 3.2.2. In Situ Major and Trace Elements of Hornblende

We performed LA-ICP-MS in situ major and trace element analyses for coarse-grained hornblende and two medium-to fine-grained hornblende particles (Figures 2c and 5, Table 3). In the chondrite-normalized REE diagram (Figure 5a), 16 analyses of hornblendes show upward convex REE patterns; LREE and medium rare earth elements (MREEs), particularly Pr, Nd, and Sm, are more enriched than HREEs. These REE patterns resemble those of hornblendes in many cumulates [47]. The primitive mantle-normalized trace element spidergram shows that the large ion lithophile elements (LILEs, such as Rb, Ba, K, Sr) are enriched, while Th, U, and HFSEs (Nb, Ta, Zr, Hf, Ti) are depleted (Figure 5b).

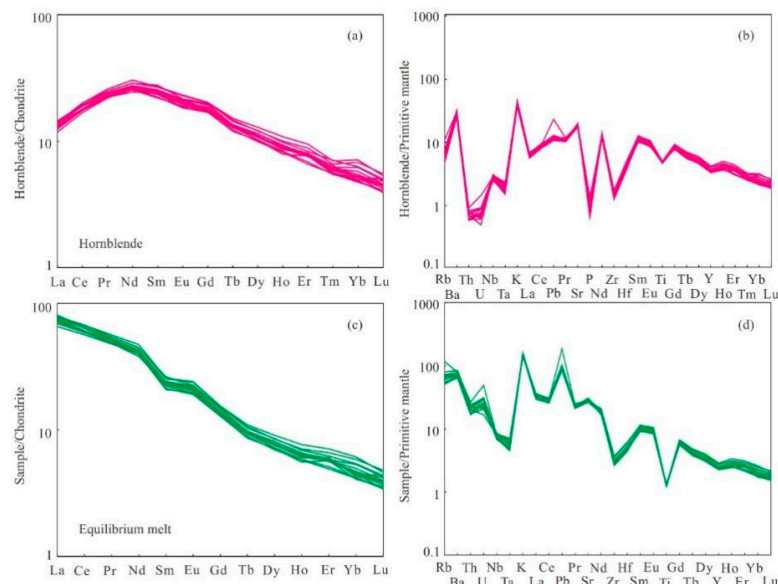


**Figure 5.** Chondrite-normalized REE patterns (a,c) [46] and primitive mantle-normalized trace element spidergrams (b,d) [48] of hornblendes from the hornblendite and their equilibrium melt.

In particular, the trace element composition of the melt in equilibrium with the hornblende from the hornblendite was calculated by applying  $\text{Am/LD}$  values experimentally determined for basaltic systems [36,37] (Table 4). Equilibrium melts show strong fractionated REE patterns, as well as strong fractionation of MREEs and HREEs, enrichment of LREEs, LILEs, U, Pb, and depletion of HREEs, Nb, Ta, Zr, Hf, and Ti (Figure 5c,d).

**Table 4.** Melt compositions (ppm) in equilibrium with the amphiboles in the Paleoproterozoic Gaositai hornblendite.

Spot No.	HB-1	HB-2	HB-3	HB-4	HB-5	HB-6	HB-7	HB-8	HB-9	HB-10	HB-11	HB-12	HB-13	HB-14	HB-15	HB-16
Ti	1652	1663	1705	1642	1666	1641	1624	1623	1661	1694	1681	1701	1654	1656	1560	1689
K	36,278	37,806	36,552	36,535	37,083	37,373	37,773	40,258	37,627	37,324	36,676	37,824	36,185	36,226	39,821	37,132
Rb	41.7	45.0	41.0	33.9	33.3	32.3	37.9	44.2	34.6	41.1	45.1	74.5	45.8	43.2	50.8	45.5
Sr	622	621	608	560	568	561	627	602	579	622	622	637	607	608	602	647
Y	11.1	10.8	10.9	11.0	11.5	10.9	11.0	12.4	13.0	12.5	11.5	10.6	10.3	10.4	10.3	11.1
Zr	32.9	32.3	32.8	29.4	31.0	31.7	35.2	40.5	41.1	39.6	35.7	34.3	33.3	35.0	36.7	35.4
Nb	5.72	5.59	5.53	4.88	5.11	5.08	5.44	6.10	5.41	5.77	5.75	5.56	5.76	5.85	5.78	5.92
Ba	475	489	512	480	465	461	495	520	449	506	527	547	537	515	586	540
La	23.7	22.6	22.3	20.3	21.5	21.5	23.3	23.4	23.3	24.3	24.4	25.0	23.5	23.0	22.8	24.3
Ce	48.7	48.3	47.4	45.6	48.1	47.5	48.6	51.7	54.1	54.4	52.7	52.5	48.5	48.4	48.4	51.1
Pr	6.02	6.02	5.91	5.83	6.31	5.97	6.25	6.63	6.85	6.62	6.42	6.31	5.89	5.92	5.98	6.16
Nd	24.9	24.0	22.8	24.2	25.1	24.4	25.0	26.7	28.3	26.8	25.7	24.6	23.7	23.9	24.0	24.5
Sm	4.48	4.33	4.43	4.48	4.67	4.46	4.51	5.11	4.98	4.94	4.70	4.65	4.05	4.14	4.32	4.60
Eu	1.54	1.50	1.52	1.62	1.64	1.56	1.53	1.65	1.77	1.75	1.63	1.59	1.46	1.40	1.43	1.51
Gd	3.53	3.42	3.34	3.53	3.86	3.64	3.56	3.91	3.99	3.98	3.77	3.46	3.33	3.32	3.46	3.48
Tb	0.45	0.46	0.44	0.44	0.46	0.45	0.45	0.50	0.52	0.49	0.46	0.44	0.41	0.44	0.42	0.46
Dy	2.43	2.48	2.47	2.44	2.59	2.47	2.50	2.72	2.91	2.75	2.60	2.42	2.30	2.32	2.24	2.51
Ho	0.46	0.43	0.45	0.46	0.47	0.46	0.45	0.51	0.55	0.50	0.47	0.44	0.40	0.42	0.41	0.45
Er	1.23	1.27	1.24	1.21	1.22	1.20	1.19	1.38	1.48	1.30	1.25	1.18	1.20	1.07	1.03	1.22
Yb	0.93	0.89	0.94	0.95	1.11	1.03	0.98	1.22	1.28	1.13	0.92	0.94	0.85	0.88	0.87	0.92
Lu	0.13	0.13	0.11	0.13	0.14	0.13	0.13	0.16	0.15	0.14	0.15	0.14	0.12	0.11	0.11	0.12
Hf	1.48	1.41	1.44	1.36	1.45	1.38	1.66	1.84	1.90	1.83	1.62	1.51	1.45	1.47	1.57	1.44
Ta	0.27	0.25	0.23	0.20	0.21	0.19	0.27	0.26	0.20	0.22	0.26	0.27	0.26	0.27	0.25	0.29
Pb	6.01	6.73	6.39	6.05	6.42	6.41	6.42	13.10	6.18	6.75	6.76	7.28	6.14	6.40	6.25	7.11
Th	1.72	1.84	1.87	1.46	1.48	1.64	1.47	1.48	1.42	1.90	1.87	2.26	2.00	1.86	2.03	1.76
U	0.35	0.48	0.62	0.51	0.63	0.54	0.43	0.55	0.52	0.44	0.47	1.03	0.65	0.63	0.63	0.64

Note:  $^{Am}/^L D$  values experimentally determined for basaltic systems are Ti 3.66, K 0.44, Rb 0.09, Sr 0.62, Y 1.39, Zr 0.45, Nb 0.34, Ba 0.37, La 0.18, Ce 0.30, Nd 0.64, Sm 1.06, Eu 0.96, Gd 1.32, Dy 1.42, Er 1.34, Yb 1.16, Lu 1.15, Hf 0.76, Ta 0.32, Pb 0.12, Th 0.03, U 0.03 [36,37], Pr 0.46, Tb 1.39, and Ho 1.42 (conjectured values of data fitting in this paper). Calculation formula is  $^{L}C = \frac{^{Am}C}{^{Am}/^L D}$ .

## 4. Discussion

### 4.1. Formation Age of the Gaositai Proterozoic Hornblendite

Early studies established the Proterozoic as the age of formation for the Gaositai ultramafic rocks in the northern NCC [31]. Recent zircon U-Pb dating studies, however, have proposed the formation ages to be in the Paleozoic and Early Mesozoic. For instance, based on the age of a gabbro dike (280 Ma), Chen et al. [33] hypothesized that the Gaositai mafic-ultramafic rocks were formed in the Early Permian, and Zhang et al. [32] determined the crystallization age of a gabbro in Gaositai to be 392 Ma through SHRIMP zircon dating. In addition, the LA-ICP-MS zircon dating for chromitite and pyroxenite indicates that the formation age was the Late Triassic (213 Ma) [35]. Several Proterozoic igneous rocks have been discovered close to the research area, including the 1894–1878 Ma Lanqi garnet granite, 1870–1819 Ma granodioritic-monzo-granites-syenogranites gneisses [9,29], the Damiao anorthosite pluton (1742–1739 Ma) [24], Lanying anorthosite and quartz syenite, and Gubeikou K-feldspar granite ( $1726 \pm 9$  Ma,  $1739 \pm 43$  Ma,  $1712 \pm 15$  Ma, and  $1692 \pm 19$  Ma) [49]. However, the question remains whether there are any Proterozoic ultramafic rocks in the Gaositai and in nearby areas.

Therefore, we conducted LA-ICP-MS zircon U-Pb dating for a hornblendite in the Gaositai ultramafic rocks. The youngest zircons in the hornblendite are euhedral to subhedral, and develop magmatic oscillatory zoning (Figure 3) and high Th/U ratios of 0.31 to 0.55, indicating that they are all products of magmatic crystallization. The dating result indicates that the youngest upper intercept age of  $1851 \pm 44$  Ma (Figure 4a) represents the forming age of hornblendite, this age is much older than the 1.7 Ga monzodiorite that intruded into the Gaositai Paleoproterozoic hornblendite and the Dantazi Group [31], our unpublished data. This Paleoproterozoic hornblendite should be separated from the Gaositai mafic–ultramafic complex that has Paleozoic zircon U-Pb ages. Thus, our study provides evidence for the presence of late Paleoproterozoic ultramafic rocks in the Gaositai area of northern Hebei; these rocks, along with the Paleoproterozoic granites, may form a bimodal igneous association. Furthermore, several 1894–1808 Ma mafic intrusive rocks also developed in southern Gaositai and in the nearby Chicheng areas [26,28], confirming the occurrence of coeval mafic magmatism in the eastern part of northern North China Craton.

On the other hand, the hornblendite samples contain three groups of magmatic captured zircons with ages of  $2206 \pm 10$  Ma,  $2399 \pm 13$  Ma, and  $2584 \pm 27$  Ma (Figure 4a). The majority of the captured zircons modified by late metamorphism still exhibit relatively obvious magmatic oscillatory zoning and REE patterns of magmatic zircons (Figures 3 and 4), which give ages that can be used to represent the formation ages of magmatic captured zircons, except for one zircon grain developing a thick zoneless metamorphic rim (2488 Ma). The coeval three stages of magmatic activity outlined above have also been found close to the study region. For instance, Feng et al. [50] reported S-type granites composed of garnet-biotite granite, garnet granite, and gneissic biotite granite in the Longhua area, which were formed at  $2180 \pm 42$  Ma. The mafic dyke swarms in the Shimen area of eastern Hebei formed at 2162 Ma in an intracontinental rift environment [51]. In addition, several 2600–2505 Ma tonalites, trondhjemites, and granodiorites, as well as 2454–2404 Ma monzogranites and migmatites, have also been identified from the Dantazi Group and the Hongqiyigzi Group [25,26,28].

### 4.2. Magma Source and Evolution

Euhedral to subhedral hornblende crystals with cumulate structure in the Gaositai Paleoproterozoic hornblendite indicate the magmatic cumulate origin. The clinopyroxene and coarse hornblende were the early-crystallizing minerals, because the fine-grained clinopyroxene inclusions formed in the core of the coarse hornblende crystal. The hornblende compositions show no large variations, and no other anhedral silicate minerals crystallized from the interstitial melt. Hence, we attempt to qualitatively estimate the composition of equilibrium magma using the trace element composition of hornblende [36,37,41].

It should be noted that both hornblende and its equilibrium melt compositions show relative enrichment in LREEs and LILEs (e.g., Rb, Ba, K, Pb), and depletion in HREEs and HSFEs (e.g., Nb, Ta, Zr, Hf, Ti), which is geochemically similar to those of the hornblendes and their host basaltic rocks in subduction zones (Figures 5 and 6). These characteristics might have been attributed to an origin of partial melting of a slab-derived fluid/melt metasomatized mantle source (Figure 6) [37,41,52–54]. Further partial melting under garnet-facies conditions comes from the observation of strongly fractionated REE and HREE patterns with lower HREE abundances in hornblende and equilibrium melt, as well as the relatively lower HREE contents in primary magmatic zircons (Figures 4 and 5) [55,56]. In addition, the extensive crystallization of hornblende indicates the primary hydrous magma source, and the presence of phlogopite also gives the most direct evidence for mantle metasomatism, which is consistent with the negative correlations of Rb/Sr and Ba/Rb in the equilibrium melt [57]. U/Th and Th/Nb for mafic rocks have generally been used to determine distinct slab-derived components metasomatized by the mantle source, because LILEs and U are easily mobilized in slab-derived fluid, while LREEs and Th are more incompatible in slab-derived melts [53,54,58]. These two values for the equilibrium melt exhibit a notable slab-derived sediment-melt signature (Figure 6) [53]. This, together with the generation of phlogopite, suggests that the mantle source was metasomatized by slab-derived K-rich silicate melts.

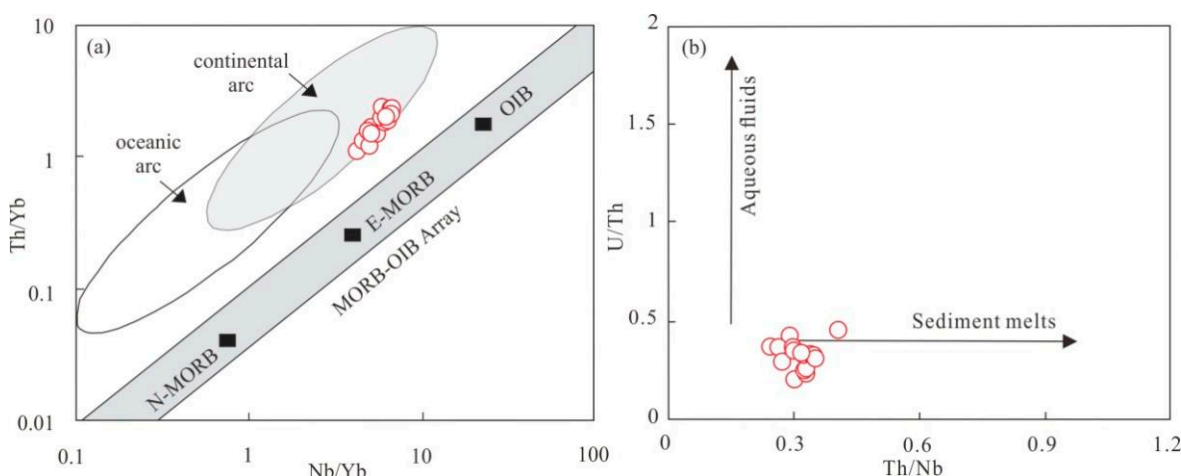


**Figure 6.** Th/Yb vs. Nb/Yb (a) [52] and U/Th vs. Th/Nb (b) [53] of equilibrium melt of hornblendes from the Paleoproterozoic Gaositai hornblende.

Before emplacement, the magma underwent multiple stages of mineral fractional crystallization. The relatively low Cr, Co, Ni contents are consistent with early fractional crystallization of olivine and clinopyroxene. The mentioned mineral inclusions, as well as core-mantle composition changes of coarse-grained hornblende, including an increase of Ti and a decrease of Mg, Al, Ca, V (Figure 7), are evidence that an early fractional crystallization of clinopyroxene + large-grained hornblende (core) occurred under the conditions of relatively high water contents [56]. Then, the dominant mantle-rim of coarse hornblende + fine-grained hornblende + magnetite + pyrite + phlogopite crystallized, which resulted in the dominant decrease of Fe in hornblende from the residual magma [37,41]. In addition, the comparatively elevated and consistent Mg, Al, Ca, V, Sr/Y, La/Yb<sub>N</sub> [48], and Dy/Yb found in late-forming hornblende rims and crystals (Figure 7), could be explained by the addition of mantle-derived magma [37]. Additionally, there is no plagioclase in hornblendite, and no obvious Eu anomaly or change in the hornblende and the equilibrium melt, indicating that there is no obvious plagioclase fractional crystallization, because the high water content of the magma suppressed the nucleation and crystallization of plagioclase [59–61].

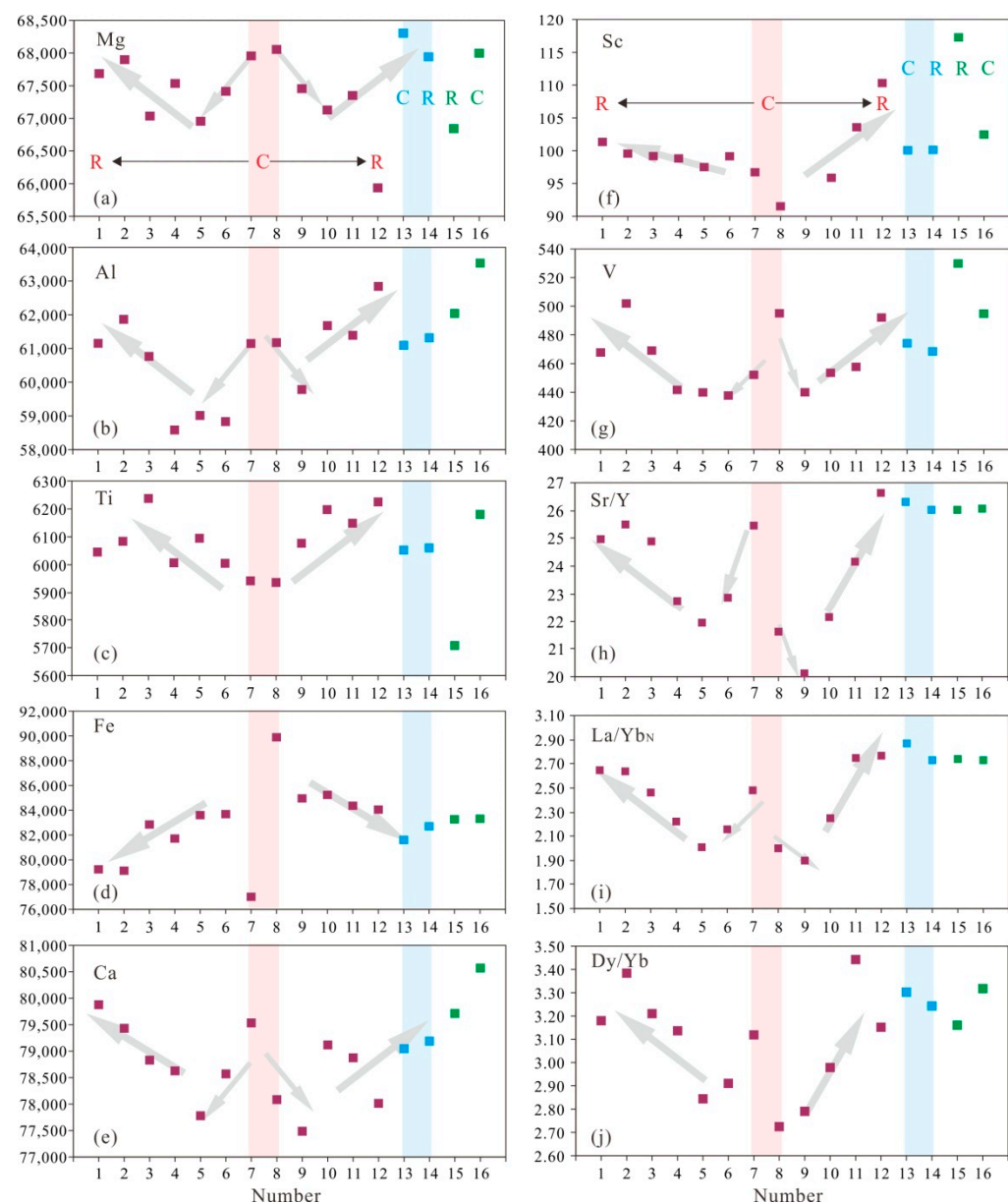


**Figure 7.** Variations of major and trace elements and ratios from core to rim (a–j) of three hornblende grains (three colors) from the Gaositai Paleoproterozoic hornblendite.

#### 4.3. Tectonic Setting and Implications

The tectonic setting of the generation of the Gaositai hornblendite is still not clear, as a result of the paucity of research on the formation of the 1.85 Ga mafic to ultramafic magmatic rocks in the study area. Thus, we use zircon trace elements and melt composition equilibrium with hornblendes to reveal the geodynamic mechanism.

Firstly, the high U/Yb and low Y concentrations of the magmatic and captured zircons in hornblendite set them apart from zircons from the oceanic crust (Figure 8a) [39]. Moreover, the presence of a large number of 2.2, 2.4, and 2.6 Ga magmatic captured zircons provides further evidence that the formation of the magmatic zircons was associated with the continental crust evolution. In addition, magmatic zircon trace elements can be used to determine the tectonic setting where magma was generated. For instance, in the U/Yb vs. Nb/Yb diagram, the magmatic zircons from MORB and OIB dominantly fall into the mantle array, and the magmatic zircons from the continental arc and post-collision rocks have relatively larger U/Yb ratios (Figure 8b) [40]. The 1851 Ma magmatic zircons from the

hornblendite plot into the overlapping zone of continental arc and post-collisional origin zircons (Figure 8b) [40].

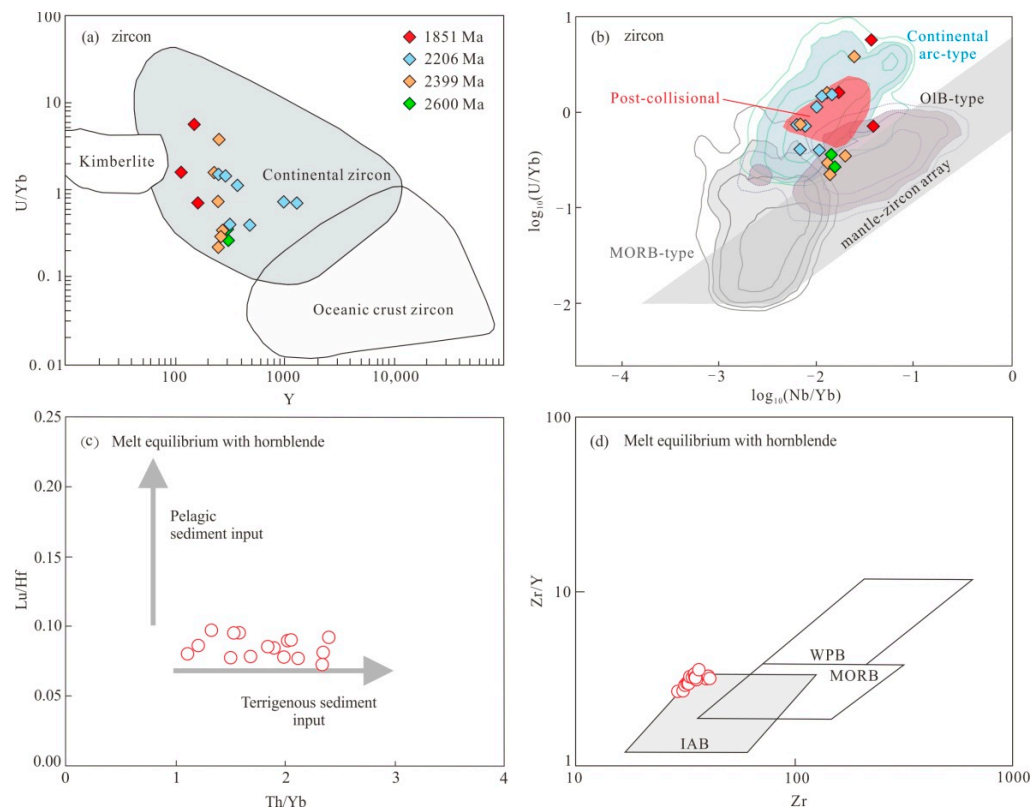


**Figure 8.** U/Yb vs. Y [39] (a), U/Yb vs. Nb/Yb [40] (b) for zircons, Lu/Hf vs. Th/Yb [53] (c), and Zr/Y vs. Zr [62] (d) for equilibrium melt of hornblendes from the Paleoproterozoic Gaositai hornblendite.

Furthermore, hornblende and equilibrium melt compositions have shown that the hornblendite magma originated from a hydrous garnet-facies mantle source metasomatized by silicate melt. Low Lu/Hf and high Th/Yb ratios of the equilibrium melt compositions indicate the addition of continental margin sediments (Figure 8c) [53]. At the same time, they show high Zr/Y, Th/Yb, Nb/Yb, and low Zr, which are similar to the characteristics of continental arc magma (Figures 6a and 8d) [52,62]. These pieces of evidence point to the melt metasomatism in the mantle source region related to the partial melting of subducted continental sediments in a continental arc environment [53,54,58]. While the aforementioned geochemical characteristics could occur in both arc mafic rocks and post-collisional mafic to ultramafic rocks, the amphibole-rich rocks were mostly produced at convergent plate margins or distributed along orogenic belts, which could have formed in the oceanic ridge subduction or post-collisional extension settings [63–66]. In general, ridge subduction produced voluminous magmatic rocks, including rock assemblages of adakite, OIB, and Nb-rich basalt [67], which are absent in the study area. On the other hand, the notably slab-derived melt metasomatism in the mantle source at least implies that the slab subduction happened before the collision to post-collisional extension. Therefore, we consider that the generation of the Gaositai Paleoproterozoic hornblendite was likely the product of the post-collisional extension mechanism, and dominantly inherited the pre-subduction mantle source.

The North China Craton was formed by the collision of eastern and western North China blocks at 1.85 Ga [4,21–24,68]. Prior to the collision process, the Paleoproterozoic subduction probably occurred along TNCO, as indicated by the presence of Paleoproterozoic Chicheng SSZ ophiolite and the Paleoproterozoic cold-subduction related eclogite facies meta-

morphism [13,30,69]. To the north of the study area, 1894–1878 Ma S-type garnet-bearing granites [29], the post-collisional 1853–1827 Ma granodiorite-monzo-granite-syenogranite intrusions, and 1742–1739 Ma Damiao anorthosite-norite-mangerite-troctolite have been recognized [9,24]. The 1853–1808 Ma gabbroic diorites and granites in the Chicheng region to the west formed in a post-collisional setting [70]. Additionally, the granulite facies metamorphism occurred in the Khondalite Belt and TNCO during 1.9–1.8 Ga [4,22,68,71]. These magmatic and metamorphic events documented the continent–continent collision between the eastern North China Block and the western North China Block, and the related post-collisional extension [4,9,22–24,29,70]. The extension process led to the asthenosphere upwelling, which triggered the partial melting of the garnet facies mantle rocks metasomatized by the slab-derived melt in the early stage. The predominant fractional crystallization and accumulation of hornblende in the underplating mafic magma beneath the lower crust resulted in the generation of late Paleoproterozoic hornblendite.

## 5. Conclusions

- (1) The Gaositai hornblendite formed at  $1851 \pm 44$  Ma, together with coeval post-collisional granites, formed a bimodal igneous assemblage.
- (2) The magma of the Paleoproterozoic phlogopite-bearing hornblendite could originate from a hydrous garnet-facies mantle source metasomatized by slab-derived silicate melt, and has undergone mineral fractional crystallization and magma recharge.
- (3) The Gaositai Paleoproterozoic hornblendite formed in the post-collisional extension setting related to the collision between the eastern and western North China blocks.

**Author Contributions:** Conceptualization, Z.W. (Zhiwei Wang); methodology, Z.W. (Zhiwei Wang); software, T.Z. and Y.S.; investigation, T.Z., Z.W. (Zhiwei Wang), J.Y. and X.G.; data curation, T.Z., Y.S., Z.L. and H.W.; writing—original draft preparation, T.Z., Z.W. (Zhiwei Wang), Z.W. (Zhihui Wang), Y.S., Z.L. and Y.X.; writing—review and editing, T.Z., Z.W. (Zhiwei Wang) and Z.W. (Zhihui Wang); visualization, Z.W. (Zhiwei Wang); supervision, Z.W. (Zhiwei Wang); project administration, Z.W. (Zhiwei Wang); funding acquisition, Z.W. (Zhiwei Wang), H.W. and X.G.. All authors have read and agreed to the published version of the manuscript.

**Funding:** This research was funded by the Science and Technology Project of the Hebei Education Department (Grant No. ZD2021015), the Science and Technology Innovation Team project of Hebei GEO University (Grant No. KJCXTD-2021-05), the Central Guidance on Local Science and Technology Development Fund (Grant No. 216Z4201G), the National Natural Science Foundation of China (Grant No. 41802053), the Natural Science Foundation of Hebei Province (grant No. D2020403019), and the Opening Foundation of Hebei Key Laboratory of Strategic Critical Mineral Resources (Grant No. HGU-SCRM2201).

**Institutional Review Board Statement:** Not applicable.

**Informed Consent Statement:** Not applicable.

**Data Availability Statement:** The data presented in this study are available in this paper.

**Acknowledgments:** We are grateful to the handling editor, and thank the two anonymous reviewers for their constructive comments. We also thank Lu Yin and Kai Xing for their help with the LA-ICP-MS analysis.

**Conflicts of Interest:** The authors declare no conflict of interest.

## References

1. Liu, D.Y.; Nutman, A.P.; Compston, W.; Wu, J.S.; Shen, Q.H. Remnants of  $\geq 3800$  Ma crust in the Chinese part of the Sino-Korean Craton. *Geology* **1992**, *20*, 339–342. [[CrossRef](#)]
2. Song, B.; Nutman, A.P.; Liu, D.; Wu, J. 3800 to 2500 Ma crustal evolution in the Anshan area of Liaoning Province, northeastern China. *Precambrian Res.* **1996**, *78*, 79–94. [[CrossRef](#)]
3. Zhao, G.C.; Sun, M.; Wilde, S.A.; Li, S.Z. Assembly, Accretion and Breakup of the Paleo-Mesoproterozoic Columbia Supercontinent: Records in the North China Craton. *Gondwana Res.* **2003**, *6*, 417–434. [[CrossRef](#)]
4. Zhao, G.C.; Zhai, M.G. Lithotectonic elements of Precambrian basement in the North China Craton: Review and tectonic implications. *Gondwana Res.* **2013**, *23*, 1207–1240. [[CrossRef](#)]
5. Zhai, M.G.; Peng, P. Paleoproterozoic events in the North China Craton. *Acta Petrol. Sin.* **2007**, *23*, 2665–2682. (In Chinese with English Abstract)

6. Zhai, M.G.; Zhu, X.Y.; Zhou, Y.Y.; Zhao, L.; Zhou, L.G. Continental crustal evolution and synchronous metallogeny through time in the North China Craton. *J. Asian Earth Sci.* **2020**, *194*, 104169. [[CrossRef](#)]
7. Wan, Y.S.; Liu, D.Y.; Song, B.; Wu, J.S.; Yang, C.H.; Zhang, Z.Q.; Geng, Y.S. Geochemical and Nd isotopic compositions of 3.8 Ga meta-quartz dioritic and trondhjemite rocks from the Anshan area and their geological significance. *J. Asian Earth Sci.* **2005**, *24*, 563–575. [[CrossRef](#)]
8. Kusky, T.M. Geophysical and geological tests of tectonic models of the North China Craton. *Gondwana Res.* **2011**, *20*, 26–35. [[CrossRef](#)]
9. Liu, S.W.; Fu, J.H.; Lu, Y.J.; Chen, X.; Wang, M.J.; Hu, F.Y.; Gao, L.; Sun, G.Z.; Hu, Y.L. Precambrian Hongqiyngzi Complex at the northern margin of the North China Craton: Its zircon U-Pb-Hf systematics, geochemistry and constraints on crustal evolution. *Precambrian Res.* **2019**, *326*, 58–83. [[CrossRef](#)]
10. Li, Z.; Chen, B.; Wei, C. Is the Paleoproterozoic Jiao-Liao-Ji Belt (North China Craton) a rift? *Int. J. Earth Sci.* **2017**, *106*, 355–375. [[CrossRef](#)]
11. Li, Z.; Chen, B.; Yan, X.L. The Liaohe Group: An insight into the Paleoproterozoic tectonic evolution of the Jiao-Liao-Ji Belt, North China Craton. *Precambrian Res.* **2019**, *326*, 174–195. [[CrossRef](#)]
12. Li, Z.; Wei, C.J.; Chen, B.; Fu, B.; Gong, M.Y. Late Neoarchean reworking of the Mesoarchean crustal remnant in northern Liaoning, North China Craton: A U-Pb-Hf-O-Nd perspective. *Gondwana Res.* **2020**, *80*, 350–369. [[CrossRef](#)]
13. Zhang, Y.Y.; Wei, C.J.; Chu, H. Paleoproterozoic oceanic subduction in the North China Craton: Insights from the metamorphic  $P-T-t$  paths of the Chicheng Mélange in the Hongqiyngzi Complex. *Precambrian Res.* **2020**, *342*, 105671. [[CrossRef](#)]
14. Bai, Y.; Su, B.X.; Xiao, Y.; Lenaz, D.; Sakyi, P.A.; Liang, Z.; Chen, C.; Yang, S.H. Origin of Reverse Zoned Cr-Spinels from the Paleoproterozoic Yanmenguan Mafic-Ultramafic Complex in the North China Craton. *Minerals* **2018**, *8*, 62. [[CrossRef](#)]
15. Zhou, Y.Y.; Zhai, M.G. Mantle plume-triggered rifting closely following Neoarchean cratonization revealed by 2.50–2.20 Ga magmatism across North China Craton. *Earth-Sci. Rev.* **2022**, *230*, 104060. [[CrossRef](#)]
16. Sun, G.Z.; Liu, S.W.; Wang, M.J.; Bao, H.; Teng, G.X. Complex Neoarchean mantle metasomatism: Evidence from sanukitoid diorites-monozodiorites-granodiorites in the northeastern North China Craton. *Precambrian Res.* **2020**, *342*, 105692. [[CrossRef](#)]
17. Sun, G.Z.; Liu, S.W.; Cawood, P.A.; Tang, M.; van Hunen, J.; Gao, L.; Hu, Y.L.; Hu, F.Y. Thermal state and evolving geodynamic regimes of the Meso- to Neoarchean North China Craton. *Nature Com.* **2021**, *12*, 3888. [[CrossRef](#)]
18. Zhai, M.G.; Liu, W.J. Palaeoproterozoic tectonic history of the north China Craton: A review. *Precambrian Res.* **2003**, *122*, 183–199. [[CrossRef](#)]
19. Zhai, M.G.; Santosh, M. The early Precambrian odyssey of the North China Craton: A synoptic overview. *Gondwana Res.* **2011**, *20*, 6–25. [[CrossRef](#)]
20. Zhai, M.G.; Li, T.S.; Peng, P.; Hu, B.; Liu, F.; Zhang, Y.B. Precambrian key tectonic events and evolution of the North China Craton. *Geol. Soc. London Spec. Publ.* **2010**, *338*, 235–262. [[CrossRef](#)]
21. Santosh, M. Assembling North China Craton within the Columbia supercontinent: The role of double-sided subduction. *Precambrian Res.* **2010**, *178*, 149–167. [[CrossRef](#)]
22. Yin, C.Q.; Zhao, G.C.; Guo, J.H.; Sun, M.; Xia, X.P.; Zhou, X.W.; Liu, C.H. U-Pb and Hf isotopic study of zircons of the Helanshan Complex: Constraints on the evolution of the Khondalite Belt in the Western Block of the North China Craton. *Lithos* **2011**, *122*, 25–38. [[CrossRef](#)]
23. Zhao, G.C.; Sun, M.; Wilde, S.A.; Li, S.Z. Late Archean to Paleoproterozoic evolution of the North China Craton: Key issues revisited. *Precambrian Res.* **2005**, *136*, 177–202. [[CrossRef](#)]
24. Zhao, T.P.; Chen, W.; Zhou, M.F. Geochemical and Nd-Hf isotopic constraints on the origin of the ~1.74-Ga Damiao anorthosite complex, North China Craton. *Lithos* **2009**, *113*, 673–690. [[CrossRef](#)]
25. Liu, S.W.; Lü, Y.J.; Feng, Y.G.; Zhang, C.; Tian, W.; Yan, Q.R.; Liu, X.M. Geology and zircon U-Pb isotopic chronology of Dantazi Complex, Northern Hebei Province. *Geol. J. China Univ.* **2007**, *13*, 484–497. (In Chinese with English Abstract)
26. Wang, F.; Chen, F.K.; Siebel, W.; Li, S.Q.; Peng, P.; Zhai, M.G. Zircon U-Pb geochronology and Hf isotopic composition of the Hongqiyngzi Complex, northern Hebei Province: New evidence for Paleoproterozoic and late Paleozoic evolution of the northern margin of the North China Craton. *Gondwana Res.* **2011**, *20*, 122–136. [[CrossRef](#)]
27. Qu, J.F.; Li, J.Y.; Liu, J.F. Geochronological study on the Fenghuangzui complex of Dantazi Group at northern Hebei Province. *Acta Petrol. Sin.* **2012**, *28*, 2879–2889. (In Chinese with English Abstract)
28. Chu, H.; Wang, H.C.; Wei, C.J.; Liu, H.; Zhang, K. The metamorphic evolution history of high pressure granulites in Chengde area, northern margin of north China: Zircon chronology and geochemical evidence. *Acta Geosci. Sin.* **2012**, *33*, 977–987. (In Chinese with English Abstract)
29. Liu, J.F.; Li, J.Y.; Qu, J.F.; Hu, Z.C.; Guo, C.L.; Chen, J.Q. Petrogenesis of Lanqizhen Paleoproterozoic garnet granite at Longhua Area in the northern margin of the North China Craton and its geological significance. *Acta Geol. Sin.* **2016**, *90*, 2365–2383. (In Chinese with English Abstract)
30. Liu, H.; Zhang, H.F. Paleoproterozoic ophiolite remnants in the northern margin of the North China Craton: Evidence from the Chicheng peridotite massif. *Lithos* **2019**, *344–345*, 311–323. [[CrossRef](#)]
31. HBGMR. *Regional Geology of Hebei Province, Beijing Municipality and Tianjin Municipality*; Geological Publishing House: Beijing, China, 1989; pp. 1–741, (In Chinese with English Abstract).

32. Zhang, S.H.; Zhao, Y.; Liu, X.C.; Liu, D.Y.; Chen, F.K.; Xie, L.W.; Chen, H.H. Late Paleozoic to Early Mesozoic mafic-ultramafic complexes from the northern North China Block: Constraints on the composition and evolution of the lithospheric mantle. *Lithos* **2009**, *110*, 229–246. [[CrossRef](#)]
33. Chen, B.; Suzuki, K.; Tian, W.; Jahn, B.M.; Ireland, T. Geochemistry and Os–Nd–Sr isotopes of the Gaositai Alaskan-type ultramafic complex from the northern North China craton: Implications for mantle–crust interaction. *Contrib. Mineral. Petrol.* **2009**, *158*, 683–702.
34. Shao, J.A.; Tian, W.; Zhang, J.H. Early Permian Cumulates in Northern Margin of North China Craton and Their Tectonic Significances. *Earth Sci. J. China Univ. Geosci.* **2015**, *40*, 1441–1457. (In Chinese with English Abstract)
35. Li, L.X.; Li, H.M.; Cui, Y.H.; Zhu, M.Y.; Wang, D.Z.; Yang, X.Q.; Liu, M.J.; Chen, J. Geochronology and petrogenesis of the Gaositai Cr-bearing ultramafic complex, Hebei Province, China. *Acta Petrol. Sin.* **2012**, *28*, 3757–3771, (In Chinese with English Abstract).
36. Tiepolo, M.; Oberti, R.; Zanetti, A.; Vannucci, R.; Foley, S.F. Trace-element partitioning between amphibole and silicate melt. *Rev. Mineral. Geochem.* **2007**, *67*, 417–452. [[CrossRef](#)]
37. Tiepolo, M.; Tribuzio, R.; Langone, A. High-Mg Andesite Petrogenesis by Amphibole Crystallization and Ultramafic Crust Assimilation: Evidence from Adamello Hornblendites (Central Alps, Italy). *J. Petrol.* **2011**, *52*, 1011–1045. [[CrossRef](#)]
38. Xie, X.F.; Yang, Z.N.; Zhang, H.; Polat, A.; Xu, Y.; Deng, X. Finding of Ca. 1.6 Ga Detrital Zircons from the Mesoproterozoic Dagushi Group, Northern Margin of the Yangtze Block. *Minerals* **2021**, *11*, 371. [[CrossRef](#)]
39. Grimes, C.B.; John, B.E.; Kelemen, P.B.; Mazdab, F.K.; Wooden, J.L.; Cheadle, M.J.; Hanghøj, K.; Schwartz, J.J. Trace element chemistry of zircons from oceanic crust: A method for distinguishing detrital zircon provenance. *Geology* **2007**, *35*, 643–646. [[CrossRef](#)]
40. Grimes, C.B.; Wooden, J.L.; Cheadle, M.J.; John, B.E. “Fingerprinting” tectono-magmatic provenance using trace elements in igneous zircon. *Contrib. Mineral. Petrol.* **2015**, *170*, 46. [[CrossRef](#)]
41. Torres García, M.F.; Calderón, M.; Ramírez de Arellano, C.; Hervé, F.; Opitz, J.; Theye, T.; Fanning, C.M.; Pankhurst, R.J.; González-Guillot, M.; Fuentes, F.; et al. Trace element composition of amphibole and petrogenesis of hornblendites and plutonic suites of Cretaceous magmatic arcs developed in the Fuegian Andes, southernmost South America. *Lithos* **2020**, *372–373*, 105656.
42. Wang, Z.W.; Wang, Z.H.; Zhang, Y.J.; Xu, B.; Li, Y.G.; Tian, Y.J.; Wang, Y.C.; Peng, J. Linking ~1.4–0.8 Ga volcano-sedimentary records in eastern Central Asian orogenic belt with southern Laurentia in supercontinent cycles. *Gondwana Res.* **2022**, *105*, 416–431. [[CrossRef](#)]
43. Liu, Y.S.; Hu, Z.C.; Zong, K.Q.; Gao, C.G.; Gao, S.; Xu, J.; Chen, H.H. Reappraisal and refinement of zircon U-Pb isotope and trace element analyses by LA-ICP-MS. *Chin. Sci. Bull.* **2010**, *55*, 1535–1546. [[CrossRef](#)]
44. Ludwig, K.R. User’s Manual for Isoplot 3.00: A Geochronological Toolkit for Excel. *Berkeley Geochronol. Cent. Spec. Publ.* **2003**, *4*, 25–32.
45. Paton, C.; Hellstrom, J.; Paul, B.; Woodhead, J.; Herdt, J. Iolite: Freeware for the visualisation and processing of mass spectrometric data. *J. Anal. At. Spectrom.* **2011**, *26*, 2508–2518. [[CrossRef](#)]
46. Boynton, W.V. Cosmochemistry of the rare earth elements: Meteorite studies. In *Rare Earth Element Geochemistry*; Henderson, P., Ed.; Elsevier: Amsterdam, The Netherlands, 1984; pp. 63–114.
47. Ma, X.; Chen, B.; Niu, X.L. Genesis of the Late Paleozoic Dongwanzi pluton, eastern Hebei. *Acta Petrol. Sin.* **2009**, *25*, 1975–1988. (In Chinese with English Abstract)
48. Sun, S.S.; McDonough, W.F. Chemical and isotopic systematics of oceanic basalts: Implications for mantle composition and processes. *Geol. Soc. London Spec. Publ.* **1989**, *42*, 313–345. [[CrossRef](#)]
49. Zhang, S.H.; Liu, S.W.; Zhao, Y.; Yang, J.H.; Song, B.; Liu, X.M. The 1.75–1.68 Ga anorthosite-mangerite-alkali granitoid-rapakivi granite suite from the northern North China Craton: Magmatism related to a Paleoproterozoic orogen. *Precambrian Res.* **2007**, *155*, 287–312. [[CrossRef](#)]
50. Feng, Y.G.; Liu, S.W.; Lü, Y.J.; Zhang, C.; Shu, G.M.; Wang, C.Q. Monazite age mapping of Longhua S-type granites in the northern margin of the North China Craton. *Acta Petrol. Sin.* **2008**, *24*, 104–114. (In Chinese with English Abstract)
51. Yang, C.H.; Du, L.L.; Geng, Y.S.; Ren, L.D.; Lu, Z.L.; Song, H.X. Paleoproterozoic metamorphic dyke swarms in the eastern Hebei massif, the eastern North China Craton: ~2.1 Ga extension and ~1.8Ga metamorphism. *Acta Petrol. Sin.* **2017**, *33*, 2827–2849, (In Chinese with English Abstract).
52. Pearce, J.A. Immobile element fingerprinting of ophiolites. *Elements* **2014**, *10*, 101–108. [[CrossRef](#)]
53. Zhao, L.; Guo, F.; Fan, W.M.; Huang, M.W. Roles of subducted pelagic and terrigenous sediments in Early Jurassic mafic magmatism in NE China: Constraints on the architecture of Paleo-Pacific subduction zone. *J. Geophys. Res. Solid Earth* **2019**, *124*, 2525–2550. [[CrossRef](#)]
54. Hawkesworth, C.J.; Turner, S.P.; McDermott, F.; Peate, D.W.; van Calsteren, P. U-Th isotopes in arc magmas: Implications for element transfer from the subducted crust. *Science* **1997**, *276*, 551–555. [[CrossRef](#)] [[PubMed](#)]
55. Martin, H. Adakitic magmas: Modern analogues of Archaean granitoids. *Lithos* **1999**, *46*, 411–429. [[CrossRef](#)]
56. Garrison, J.M.; Davidson, J.P. Dubious case for slab melting in the Northern volcanic zone of the Andes. *Geology* **2003**, *31*, 565–568. [[CrossRef](#)]
57. Furman, T.; Graham, D. Erosion of lithospheric mantle beneath the East African Rift system: Geochemical evidence from the Kivu volcanic province. *Lithos* **1999**, *48*, 237–262. [[CrossRef](#)]

58. Xiao, Y.Y.; Niu, Y.L.; Wang, K.L.; Lee, D.C.; Iizuka, Y. Geochemical behaviours of chemical elements during subduction-zone metamorphism and geodynamic significance. *Int. Geol. Rev.* **2016**, *58*, 1253–1277. [[CrossRef](#)]
59. Beard, J.S.; Lofgren, G.E. An experiment-based model for the petrogenesis of high-alumina basalts. *Science* **1992**, *258*, 112–115. [[CrossRef](#)]
60. Sisson, T.W.; Grove, T.L. Temperatures and H<sub>2</sub>O contents of low-MgO high-alumina basalts. *Contrib. Mineral. Petrol.* **1993**, *113*, 167–184. [[CrossRef](#)]
61. Grove, T.L.; Till, C.B.; Krawczynski, M.J. The role of H<sub>2</sub>O in subduction zone magmatism. *Annu. Rev. Earth Planet. Sci.* **2012**, *40*, 413–439. [[CrossRef](#)]
62. Pearce, J.A.; Norry, M.J. Petrogenetic implications of Ti, Zr, Y, and Nb variations in volcanic rocks. *Contrib. Mineral. Petrol.* **1979**, *69*, 33–47. [[CrossRef](#)]
63. Thorkelson, D.J.; Breitsprecher, K. Partial melting of slab window margins: Genesis of adakitic and non-adakitic magmas. *Lithos* **2005**, *79*, 25–41. [[CrossRef](#)]
64. Dai, L.Q.; Zhao, Z.F.; Zheng, Y.F.; Zhang, J. The nature of orogenic lithospheric mantle: Geochemical constraints from postcollisional mafic-ultramafic rocks in the Dabie orogen. *Chem. Geol.* **2012**, *334*, 99–121.
65. Murphy, J.B. Appinite suites: A record of the role of water in the genesis, transport, emplacement and crystallization of magma. *Earth-Sci. Rev.* **2013**, *119*, 35–59. [[CrossRef](#)]
66. Yuan, L.L.; Zhang, X.H.; Zhai, M.G.; Xue, F.H. Petrogenesis and geodynamic implications of appinite suite. *Acta Petrol. Sin.* **2016**, *32*, 1556–1570, (In Chinese with English Abstract).
67. Wang, Q.; Tang, G.J.; Hao, L.L.; Wyman, D.; Ma, L.; Dan, W.; Zhang, X.Z.; Liu, J.H.; Huang, T.Y.; Xu, C.B. Ridge subduction, magmatism, and metallogenesis. *Sci. China Earth Sci.* **2020**, *63*, 1499–1518. [[CrossRef](#)]
68. Zhao, G.C.; Cawood, P.A.; Li, S.Z.; Wilde, S.A.; Sun, M.; Zhang, J.; He, Y.H.; Yin, C.Q. Amalgamation of the North China Craton: Key issues and discussion. *Precambrian Res.* **2012**, *222–223*, 55–76. [[CrossRef](#)]
69. Tian, W.; Wang, S.Y.; Liu, F.L.; Chu, Z.Y.; Wang, B.; Chen, M.M.; Prichard, J. Archean-Paleoproterozoic Lithospheric Mantle at the Northern Margin of the North China Craton Represented by Tectonically Exhumed Peridotites. *Acta Geol. Sin.* **2017**, *91*, 2041–2057. [[CrossRef](#)]
70. Wang, F.; Peng, P.; Chen, C.; Hu, H.F.; Huang, D.Q.; Chen, F.K.; Zhai, M.G. Petrogenesis and geological significance of the Paleoproterozoic Dushikou metagabbro-diorite in northern Hebei Province. *Acta Petrol. Sin.* **2021**, *37*, 269–283 (In Chinese with English Abstract)
71. Dong, X.J.; Xu, Z.Y.; Liu, Z.H.; Sha, Q. Zircon U–Pb geochronology of Archean high-grade metamorphic rocks from Xi Ulanbulang area, central Inner Mongolia. *Sci. China Earth Sci.* **2012**, *55*, 204–212. [[CrossRef](#)]